ACS APPLIED MATERIALS & INTERFACES

Research Article

www.acsami.org

Rational Design of Void-Involved Si@TiO_2 Nanospheres as High-Performance Anode Material for Lithium-Ion Batteries

Shan Fang, Laifa Shen, Guiyin Xu, Ping Nie, Jie Wang, Hui Dou, and Xiaogang Zhang*

College of Materials Science and Engineering, Key Laboratory for Intelligent Nano Materials and Devices of Ministry of Education, Nanjing University of Aeronautics and Astronautics, Nanjing, 210016, P.R. China

Supporting Information

ABSTRACT: A unique core−shell structure of silicon@titania (Si@TiO_2) composite with silicon nanoparticles encapsulated in TiO_2 hollow spheres is synthesized by a simple hydrolysis method combined with magnesiothermic reduction method. It is found that the TiO_2 shell is effective for improving the electrical conductivity and structural stability. More importantly, the well-designed nanostructure with enough empty space would accommodate the volume change of silicon during the cycling. Reversible capacities of 1911.1 and 795 mAh g^{-1} can be obtained at 0.05 C and a high current rate of 1 C, respectively. After 100 cycles at 0.1 C, the composite electrode still maintains a high capacity of 804 mAh g^{-1}. This excellent cycling stability and high-rate capability can be ascribed to the unique core−shell nanostructure and the synergistic effect between Si and TiO_2.

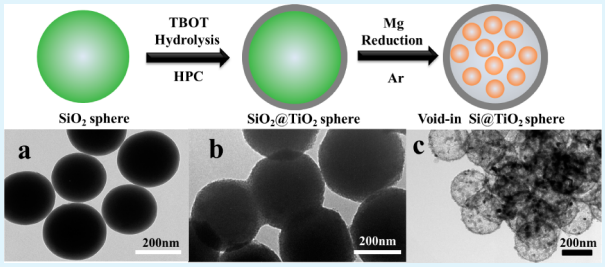

KEYWORDS: *silicon, titanium dioxide, core−shell structure, Li-ion batteries, anode*

INTRODUCTION

In the development of rechargeable lithium ion batteries, which have high energy capacity, long cycle life, and fast charge/discharge rates, is of great technology importance for energy applications, such as hybrid electric vehicle and portable electronic devices. To meet this requirement, a great deal of efforts has been devoted to develop innovative battery materials to replace the graphite anode materials in Li-ion batteries that allow a high specific capacity.[1−6] Silicon (Si) has attracted remarkable attention as an alternative anode material for Li-ion batteries, primarily because of its high theoretical capacity (4200 mAh g^{-1}), low Li-uptake voltage, low cost and ready abundance.[7−11] However, the large volume changes (300%) upon lithium insertion in Si, which results in poor capacity retention to make it difficult to practical application. This volume change causes pulverization of Silicon and thus a loss of electrical contact between Si and the current collectors, and the exposed fresh silicon surfaces to the electrolyte could also causes continual formation of unstable solid electrolyte interphase (SEI). All those undesirable factors lead to rapid capacity fading.[12−16] Encapsulating the silicon in conductive coating layers is one of the most effective strategies to tackle these volume change caused interfacial and structural instability problems of Si[17−19] and to design the silicon structures, such as nanospheres,[20] nanotubes,[21−23] and nanowires,[24,25] which have been explored previously. Although the choice of coating materials was limited by the low working potential of the anode, some coatings, such as metallic coatings and amorphous carbon, both of them have great chemical stability. However, the large volume changes of silicon during charge and discharge would destroy these coating materials, and expose the surface of silicon to the electrolyte.

Recently, Si nanostructures with void-containing have been reported as superior anode materials,[26,27] and arouse considerable interest. For example, Li and co-workers have synthesized void-involved silicon/carbon nanohybrids as anode materials.[21] Cui et al. have engineered a void space between Si particles by encapsulating them in hollow carbon tubes for stabilized and scalable silicon anodes.[8] They all show the excellent rate capability and stable cycle performance. However, both of them use carbon as coating material, and the nanostructures are prepared by chemical vapor deposition (CVD) or electrospinning method, which is expensive or complicated. Titanium-based compounds are promising candidates as coating materials like carbon.[28−31] Because of the lithiated TiO_2 layer during discharge could promote the electrical conductivity,[32,33] and the volume expansion upon lithiation is less than 4%.[34] Furthermore, the lithiated TiO_2 could also act as a physical interfacial layer because of the well noted thermal stability, suppressing exothermic reactions between the highly lithiated silicon phase and the electrolyte solution.[29] Thus, TiO_2 coated on the Si nanoparticles is potentially beneficial for both structural integrity, as well as the electrochemical performance of the composite.

Taking advantages of the void-containing structure and a stable metallic oxide coating on the electrode materials, a unique core−shell nanostructure has been designed for a

Received: January 4, 2014
Accepted: April 8, 2014
Published: April 8, 2014

   dx.doi.org/10.1021/am500066j | ACS Appl. Mater. Interfaces 2014, 6, 6497−6503

scalable and stabilized Si anode by a simple hydrothermal method combined with magnesiothermic reduction for SiO_2@TiO_2 composite. The multiple Si nanoparticles with a diameter around 10 nm were encapsulated in a thin hollow titanium dioxide spheres, and the shell thickness is about ~10 nm, which thus improved the void volume and the content of silicon in titanium dioxide shell. This unique core−shell nanostructure shows an excellent rate capability and a significantly improved cycling performance.

EXPERIMENTAL SECTION

Materials Synthesis. *Fabrication of SiO_2 Spheres.* The synthesis of SiO_2 spheres method is according a literature.[35] In brief, 3.14 mL of $NH_3{\cdot}H_2O$ solution (25%), 74 mL of absolute ethanol, and 10 mL of deionized water (DI) were mixed together, stirred for 30 min, and then added the solution with 6 mL of tetraethylorthosilicate (TEOS). Finally, it was stirred for another 6 h.

Synthesis of Si@TiO_2 and Si Spheres. The TiO_2 shell was deposited on the SiO_2 spheres by the hydrolysis of tetrabutylorthotitanate ($Ti(OC_4H_9)_4$, TBOT). Typically, 150 mg of SiO_2 spheres, 0.2 mL of DI water, 50 mg of hydroxypropyl cellulose (HPC), and 30 mL of ethanol were mixed under vigorous magnetic stirring. TBOT (0.3 mL) was dissolved in 4 mL of ethanol and then added into the system in 20 min. The solution was heated at reflux at temperature of 85 °C for 90 min. The product was washed with DI water and ethanol several times, and dried at 60 °C for 12 h. For magnesiothermic reduction reaction, 0.15 g magnesium powder (99.9%, Aladdin) and 0.15 g SiO_2@TiO_2 composite was ground in an agate mortar to form a homogeneous mixture, and then move to a tube furnace. The reduction was carried out at temperature of 650 °C for 10 h under argon atmosphere. The collected black powder was then dipped into 1 M HCl solution for 5 h to selectively remove MgO. Finally, the powder was washed by DI water and dried at 60 °C for overnight. The bare Si spheres were fabricated by direct magnesiothermic reduction of SiO_2 spheres at 650 °C for 6 h, according to the same preparation procedure for Si@TiO_2. The gravimetric capacity was based on the total mass of the Si@TiO_2 composite.

Characterization. Morphologies of the samples were characterized by scanning electron microscopy (SEM, HITACHI S-4800) and energy-dispersive X-ray spectroscopy (EDX, Phoenix), transmission electron microscopy (TEM, JEOL JEM-2010). The crystal structure was characterized by X-ray diffraction (XRD) (Bruker D8 advance) with Cu Kα radiation. Brunauer−Emmett−Teller (BET) surface area and pore size distributions were obtained from the N_2 adsorption/desorption isotherms recorded at 77 K (QUADRASORB SI, Quantachrome Instrument Corporation).

Electrochemical Test. Electrochemical evaluations were tested by galvanostatic charge/discharge in a CR2016-type coin cell. Si@TiO_2 composite, carbon black and polyvinylidene fluoride (PVDF) binder in a weight ratio of 6:2:2 were mixed, which dissolved in *N*-methylpyrrolidinone (NMP), the slurry was coated on a foil copper current collector formed as a working electrode. Then the electrodes were dried in a vacuum oven at 110 °C for overnight. The mass of active material loaded on electrode was 0.5−0.7 mg. The cells were assembled with lithium metal as the counter electrode, the separator is polypropylene film. The electrolytes were 1 mol L^{-1} $LiPF_6$ solution in a mixture of ethylene carbonate (EC) and dimethyl carbonate (DMC) (1:1, by volume). The 2016 cells were assembled inside an argon-filled glovebox. Galvanostatically charge/discharge experiments were tested at the potential range of 0.01−2.5 V (vs Li/Li^+) using a CT2001A cell test instrument (LAND Electronic Co.). An electrochemical workstation (CHI660) was used to study the cyclic voltammetry (CV) performance in the potential range of 0.05−2.5 V at a scan rate of 0.1 mV s^{-1}. Electrochemical impedance spectroscopy (EIS) was measured in the frequency between 100 kHz and 0.01 Hz and the amplitude is 5 mV.

RESULTS AND DISCUSSION

The unique core−shell structure of Si@TiO_2 was prepared by in situ reducing of SiO_2@TiO_2 composite via a simple magnesiothermic reduction method under Ar atmosphere. Figure 1 showed the synthetic procedure. In brief, SiO_2 spheres

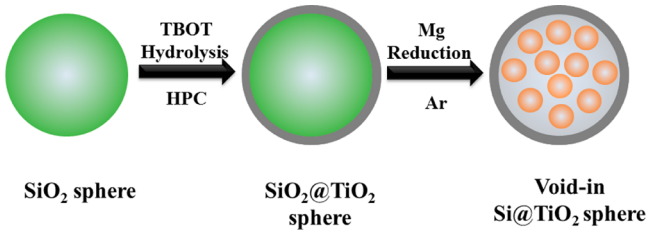

Figure 1. Schematic illustration for the fabrication process of the unique core−shell nanostructure of the Si@TiO_2 composite.

were first fabricated by the Stöber method and used as both template and silicon source. Then, the TiO_2 was coated on the surface of SiO_2 spheres to form a uniform shell by hydrolysis of TBOT. It should be noted that the TiO_2 coating shell can be controlled through adjusting the reaction time and the TBOT concentration. The reduction of the SiO_2 was conducted by magnesiothermic reduction method. The SiO_2@TiO_2 powder was homogeneous mixed with magnesium powder before pyrolysis in Ar atmosphere. After heating treatment, the powder was immersed in HCl to remove magnesia, magnesium silicide and the redundant magnesium. Finally, the silicon encapsulated in the TiO_2 hollow spheres was obtained. Here, the synthesis method is scalable, and the powder-like products also can be applied to the current slurry coating technology.

The morphology of SiO_2 nanospheres and SiO_2@TiO_2 are investigated by scanning electron microscopy (SEM) and transmission electron microscopy (TEM), respectively. A panoramic view of the as synthesized SiO_2 and SiO_2@TiO_2 revealed that the spheres were quite uniform with a diameter of 250−300 nm (Supporting Information (SI), Figure S1). The structure of Si particles and Si@TiO_2 composite are characterized by SEM and TEM. The SEM image in Figure 2a shows the image of the electrode from Si spheres without coating TiO_2. It shows that the spherical Si particles are monodisperse. This demonstrates that the spheres are composed of silicon nanocrystals, and the average diameter is 10 nm, which is further testified by TEM characterization (inset of Figure 2b). Figure 2c and 2d show the morphology of Si@TiO_2. The difference between them is that these spheres present the smooth surface and the spheres are connected. In the SEM image, very few of TiO_2 small particles could be observed, indicating that a uniform shell of TiO_2 may formed. In order to get insight into the composite structure, the sample is carried out with TEM techniques (Figure 2e and f). The core−shell structure is well confirmed by TEM analysis, between the core and the shell, there have a distinct void space existed. The thickness of the TiO_2 shell is estimated to be ca. 10 nm. It can be observed that many silicon nanoparticles are embedded in the hollow spheres. We believe that the void space inside the nanosphere can accommodate the expansion/contraction of the active materials during lithiation/delithiation processes, and the hollow structures are valid on confining active composites to reduce their diffusion into the electrolyte or contact with the electrolyte. This unique core−shell

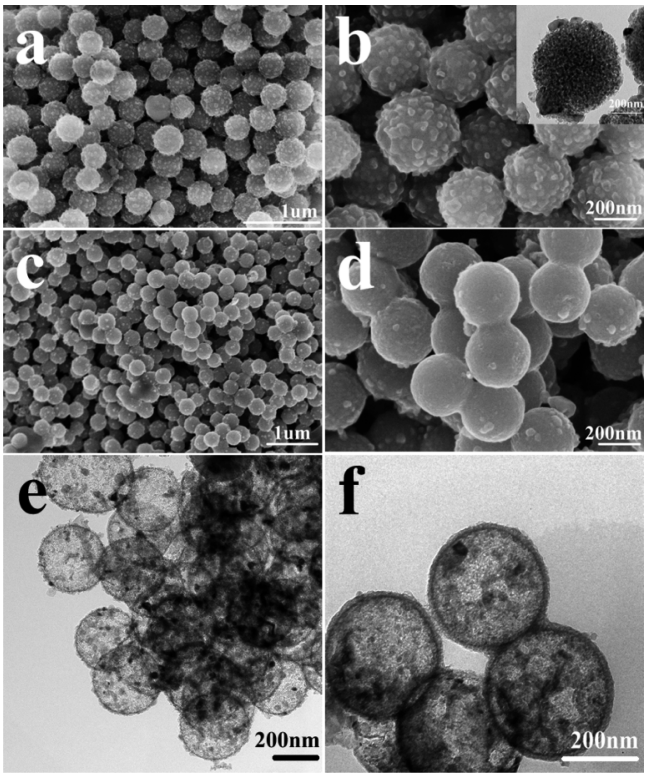

Figure 2. SEM images of Si nanospheres (a, b), Si@TiO_2 core–shell nanospheres (c, d), and TEM images of Si@TiO_2 (e, f).

structure would make good contribution to the excellent electrochemical performance for the Si@TiO_2 composite.

From Figure 3a and b, high-resolution TEM (HRTEM) images revealed that Si nanocrystals were homogeneously embedded in TiO_2 hollow spheres with the shell thickness about 10 nm (Figure 3a). From HRTEM images of TiO_2 shell, the lattice fringes in the different regions (SI Figure S2) were

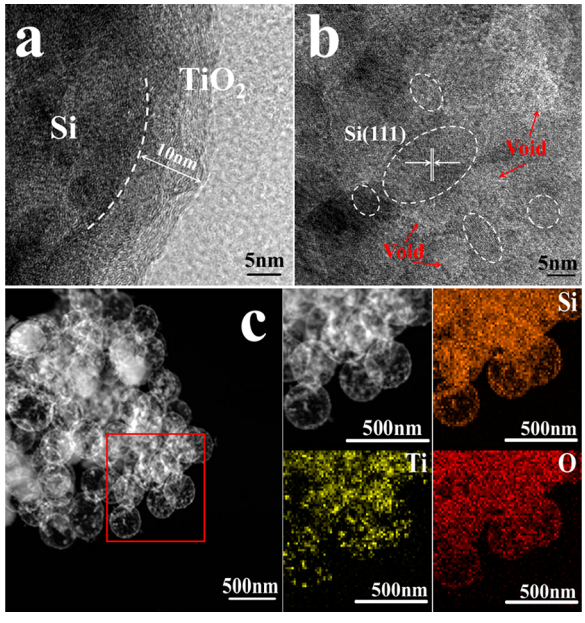

Figure 3. (a, b) HRTEM images of Si@TiO_2 and (c) STEM image and corresponding EDS mapping images of Si (orange), Ti (yellow), and O (red).

found to be ~0.315, 0.244, and 0.213 nm, respectively, indicating that it was crystalline. In Figure 3b, the crystalline lattice can be clearly observed and correspond to the (111) plane of cubic Si, the nanopores were homogeneously embedded in the spheres. Further evidence for this unique nanostructure of Si nanoparticles encapsulated by TiO_2 hollow spheres is identified by EDX mappings and the dark-field scanning transmission electron microscopy (STEM) image (Figure 3c). The results confirmed that TiO_2 shells indeed wrapped the Si nanoparticles. The elemental mapping images of silicon, titanium, and oxygen clearly demonstrate the Si nanoparticles is homogeneous distribution in the TiO_2 hollow spheres, which insures intimate contact between the Si and the TiO_2. X-ray diffraction (XRD) experiments were carried out to make clear the structure and composition of the above samples. From the XRD patterns of the samples shown in Figure 4, both

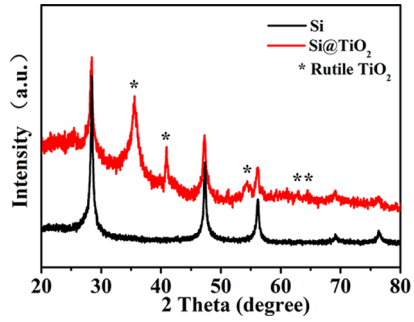

Figure 4. XRD patterns of the Si (black) and Si@TiO_2 (red) formed after Mg reduction.

Si and Si@TiO_2 particles have the major identified peaks at 2θ = 28.3, 47.3, 56.0, 69.1, 76.3°, indexed as (111), (220), (311), (400), and (331) planes of cubic silicon (JCPDS 27-1402), respectively. This confirms the transformation of SiO_2 into Si via the magnesiothermic reduction method. There is also another five peaks appeared in the pattern of Si@TiO_2, which correspond to the rutile phase of TiO_2 (JCPDS No. 21-1276). Comparison with XRD pattern of SiO_2@TiO_2 (SI Figure S3), it indicated that TiO_2 coatings could transition from amorphous to rutile after pyrolysis. As the peaks corresponding to rutile TiO_2 (110) plane lie very close to those of Si (111) plane, the observed peak at 28.3° should be corresponding to multiple planes, and the HRTEM of TiO_2 has demonstrated it (SI Figure S2).[36] N_2 adsorption–desorption measurement was carried on the Si@TiO_2 sample to understand the properties of surface area and porous structure (SI Figure S4). From the isotherm curve, a distinct hysteresis loop at the high relative pressure region can be observed, indicating the existence of the mesoporous and microporous.[37] The Brunauer–Emmett–Teller (BET) analysis reveals a specific surface area of 229.8 $m^2\ g^{-1}$ for Si@TiO_2 (SI Figure S4a). The relative high surface area of the composite is very important for active materials to participate in the reaction and a large particles-electrolyte interface to promote fast intercalation of Li-ion into Si to improve the rate performance even at high current density. The Barrett–Joyner–Halenda (BJH) pore-size distribution shows that Si@TiO_2 exhibit an average pore size around 4.07 nm in diameter, which is consistent with the above TEM and HRTEM.

dx.doi.org/10.1021/am500066j | ACS Appl. Mater. Interfaces 2014, 6, 6497–6503

The electrochemical reaction mechanism of Li with TiO_2 and Si has been well investigated and can be described by the following equations:

$$4.4Li + Si \leftrightarrow Li_{4.4}Si \quad (1)$$

$$xLi^+ + xe^- + TiO_2 \leftrightarrow Li_xTiO_2 \quad (0 \le x \le 1) \quad (2)$$

Cyclic voltammetry (CV) were tested on a half-cell in a potential range between 0.05 and 2.5 V versus Li/Li^+ at a scanning rate of 0.1 mV s^{-1} (Figure 5). The CV curves of Si@TiO_2 electrode show distinct peaks related to the specific lithiation or delithiation steps corresponding to Si and TiO_2. In the first cycle, the peak at 0.73 V in the cathodic process corresponds to the formation of SEI layers, which disappeared in the second cycle.[38] The sharp reduction peak appears at 0.19 V, representing the lithium reaction with Si. After that, two anodic peaks were observed at 0.31 and 0.50 V. These three redox peaks are correspond to the lithiation/delithiation process of Li with active silicon particles and maintaining stable (eq 1). Moreover, in the profile of Si@TiO_2 composites, redox peaks of TiO_2 appear simultaneously. Compared with the CV curve of pure TiO_2 electrode (SI Figure S5), peaks showing in the cathodic sweep range of 1.1−2.0 V, the anodic around 1.98 and 1.0 V are attributed to the lithiation/delithiation of TiO_2 (eq 2).[31] More than one redox peaks of TiO_2 could be observed which may be ascribed to the polycrystalline of the shell layer, but the low quantity and well dispersed throughout the composite make it not to be observed in the XRD pattern of Si@TiO_2 composite. It is worth noting that the peak of 1.55 V disappears in the rest cycles possibly because of the large irreversible capacity loss of TiO_2 in the first cycle. This figure displays the typical Si lithiation/delithiation behavior, which is consistent with previous reported CV curves for Si@TiO_2 composite.[34]

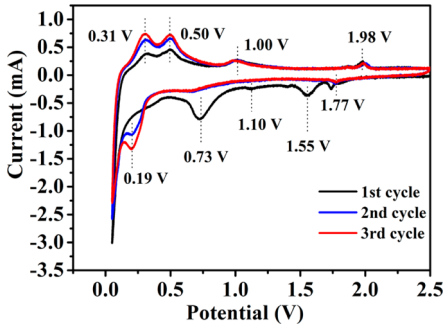

Figure 5. Cyclic voltammetry of Si@TiO_2 nanospheres from 0.05 to 2.5 V at a scan rate of 0.1 mV s^{-1}.

The well-designed and synthesized the unique core−shell nanostructure for stabilized anode is confirmed by the outstanding electrochemical performance. Figure 6a shows the 1st, 2nd, 10th, 30th, and 50th charge and discharge profile of Si@TiO_2 electrode at a current density of 0.1 C rate in potential range between 0.01 and 2.5 V (vs Li/Li^+). In the voltage profiles of the first lithiation cycle shows the differences in the electrochemical response of the TiO_2 coatings. The rutile coating clearly shows a small plateau around 1.55 V, which disappeared in the rest curves, this phenomenon may be ascribed to the irreversible lithium intercalation into TiO_2 below 1 V and it is in accordance with previous electrochemical studies on these different forms of TiO_2.[39,40] The subsequent slope at about 0.75 V can be assigned to the formation of SEI layer. The discharge plateau at approximately 0.2 V corresponds to the generation of several Li_xSi ($0 \le x \le 4.4$) alloys. The Si@TiO_2 composite has a discharge capacity of 3150 mAh g^{-1} and a charge capacity of 1671 mAh g^{-1} with Columbic efficiency (CE) at 53.1%. The irreversible capacity in the first cycle is owing to three aspects: (1) the formation of a SEI film because of electrolyte decomposition on electroactive materials, (2) the irreversible storage of Li on the rutile coating surface,[41−43] and

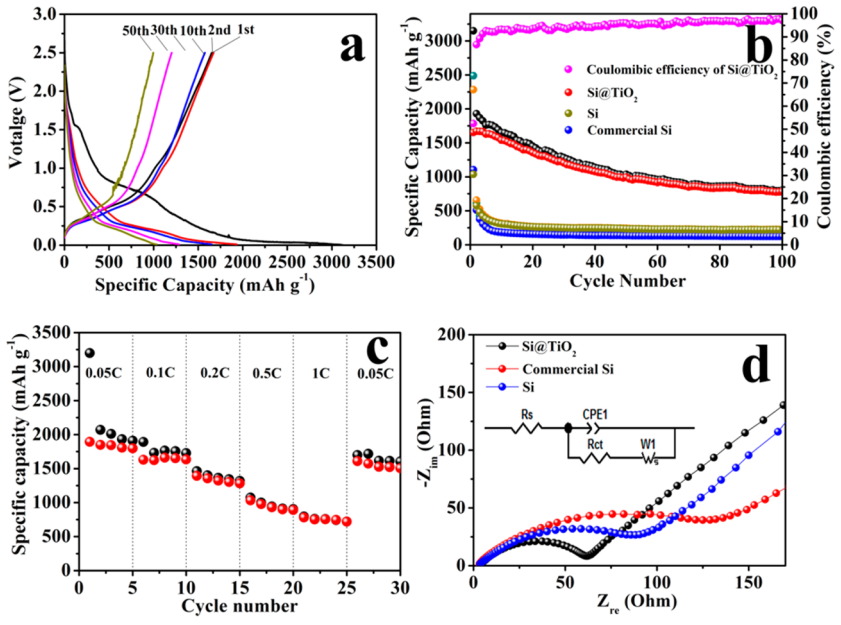

Figure 6. (a) Charge and discharge voltage profiles of Si@TiO_2 composite for 1, 2, 10, 30, and 50 cycles tested between 0.01 and 2.5 V at a rate of 0.1 C. (b) Cycling behaviors of Si@TiO_2 composite, Si reduced from SiO_2 and commercial Si at a current density of 0.1 C. (c) Rate capabilities of Si@TiO_2 composite at different C-rates. (d) Electrochemical impedance spectra of Si@TiO_2 composite, Si reduced from SiO_2 and commercial Si electrodes after 100 cycles at 0.1 C.

dx.doi.org/10.1021/am500066j | ACS Appl. Mater. Interfaces 2014, 6, 6497−6503

(3) irreversible lithium alloyed with Si. It should be noted that the specific capacity is calculated based on the total mass of Si@TiO_2, in which TiO_2 constitutes ~40% of the mass (as theoretical calculated by the shell thickness and core diameter, which can be seen in Supporting Information). CE becomes stable and larger than 92% after the fourth cycle. The Si@TiO_2 electrode displays excellent cycling performance and maintains a reversible discharge capacity of 804 mAh g^{-1} after 100 cycles, which is two times higher than the theoretical capacity of graphite. At the same time, Si spheres synthesized by direct magnesiothermic reduction of SiO_2 and commercial Si nanoparticles were also tested in Li-ion batteries as comparison samples. In the case of the bare Si electrode, the initial specific capacity reached up to 2283 mAh g^{-1} at a current density of 0.1 C (Figure 6b). However, a rapid capacity fade was observed upon further cycling. This can be attributed to the expansion/contraction of silicon during the charge and discharge, which results in the pulverization and disruption of the microstructure of the electrode. In addition to that, we also choose the commercial Si as comparison. The commercial Si nanoparticles show the worse cycling performance, and display a rapid decay of discharge capacity from 2489 to 124 mAh g^{-1} after 100 cycles at a current density of 0.1 C rate. This investigation for the unique core−shell nanostructure and TiO_2 coating material provides good mechanical properties, attenuating the volume expansion of Si nanoparticles and maintaining the structural integrity of the electrode network during the cycling. Furthermore, a rate test was carried out to investigate the transport properties of the TiO_2 coatings. The composite shows excellent rate capability (Figure 6c). The capacity decreases gradually with the increasing current density from 0.05 to 1 C. Impressively, the capacity recovers to 1700 mAh g^{-1} reversibly after the current density returns to 0.05 C rate. This phenomenon indicates the good reversibility of the electrode. To analyze the part of the total capacity due to the TiO_2 component, we hypothesis the reversible capacity of TiO_2 is 175 mAh g^{-1} at 0.05 C, the mass percent of the TiO_2 in the composite is less than 40%, indicating that the TiO_2 makes contribution to the total specific capacity of the composite electrode is about 4.12%. The Si@TiO_2 composite outperforms many other TiO_2 coating materials in electrochemical performance.[33,34] EIS technique is also utilized to clarify the remarkable electrochemical performance of Si@TiO_2 composite compared with Si spheres and commercial Si nanoparticles (Figure 6d). The corresponding equivalent circuit is presented insets of Figure 6d. The charge-transfer resistance (R_{ct}) parameters of the bare Si electrodes are obviously lager than that of the Si@TiO_2 composite electrode after the 100 cycles at rate of 0.1 C, which indicates it has higher electrical conductivity than that of the bare Si electrodes. This difference may be due to the uniform TiO_2 shell maintains their structural integrity and the lithiated TiO_2 coatings enchance the electronic conductivity of the whole electrode.

The excellent cycle performance and rate capability of the Si@TiO_2 electrode benefit from the following factors. First, the designed void spaces in TiO_2 hollow spheres allow inner Si nanoparticles to expand freely but not destroying the TiO_2 coating shell. Second, the thermostable lithiated TiO_2 is assumed to be ionic and electrical conducting, which enables the formation of efficient and robust channels for the fast-diffusion of the Li-ions and electrons to silicon nanoparticles. Finally, the TiO_2 shell as a protect layer avoids the exposure of silicon nanoparticles to the electrolyte decomposition.

The microstructural properties of the Si@TiO_2 nanocomposite electrodes were characterized by using SEM to verify the unique core−shell structure which provide more voids and pores for accommodation of volume expansion, as well as the TiO_2 shell encapsulate the Si particles maintains their structural integrity. Figure 7a and 7b present SEM images of the nanocomposite before and after 60 cycles, respectively. Compared with the image of the pristine sample, the Si@TiO_2 electrode still retained a similar surface morphology, and very few cracked spheres have been observed. Obviously, the good stability of the structure will lead to a long stable cycling performance.

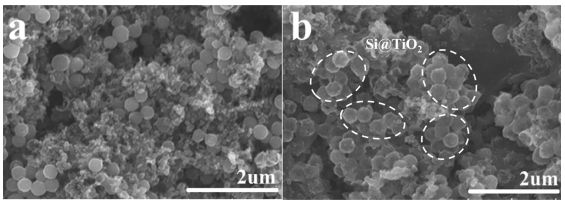

Figure 7. SEM images of the Si@TiO_2 composite before (a) and after (b) 60 charge/discharge cycles at 0.1 C.

CONCLUSIONS

In conclusion, a void-involved Si@TiO_2 nanocomposite had been rationally designed and synthesized by encapsulating of the Si nanoparticles in the hollow TiO_2 spheres. The in situ reduction of SiO_2@TiO_2 composite by using a magnesiothermic reaction is simple and fast, which enables a cost-effective and large-scale production. The significant improvement of electrochemical performance can be obtained compared to pure Si. A high reversible capacity of about 1700 mAh g^{-1} can be obtained at the current density of 0.05 C, and the capacity maintains approximately 804 mAh g^{-1} even after 100 cycles at a rate of 0.1 C. The improved performance can be ascribed to the unique core−shell hybrid structure. Rationally designed void space can right accommodate the volume change of Si without disrupting the SEI film on the surface of the shell or fracturing the TiO_2 coating layer. The synergistic between TiO_2 shell and Si nanoparticles is of great importance. In addition to Si, the TiO_2 coating could be an alternative or supplementary coating material to carbon and this unique nanostructure can also applied to other high capacity materials which have large volume changes for lithium ion batteries to promote the Coulombic efficiency and cycle performance.

ASSOCIATED CONTENT

Supporting Information

Additional SEM and TEM images, XRD pattern result, BET analysis, CV profile, and theoretical calculation of the composite. This material is available free of charge via the Internet at http://pubs.acs.org.

AUTHOR INFORMATION

Corresponding Author

*Tel.: +86-025-5211291 8. Fax: +86-025-52112626. E-mail: azhangxg@nuaa.edu.cn.

Notes

The authors declare no competing financial interest.

■ ACKNOWLEDGMENTS

This work was supported by the National Basic Research Program of China (973 Program) (No. 2014CB239701), National Natural Science Foundation of China (No. 21103091, 21173120, 51372116), Natural Science Foundation of Jiangsu Province (BK2011030), and Fundamental Research Funds for the Central Universities (NP2014403) and the Fundation of Graduate Innovation Center in NUAA (kfjj130124).

■ REFERENCES

(1) Armand, M.; Tarascon, J. M. Building Better Batteries. *Nature* **2008**, *451*, 652−657.
(2) Deng, D.; Kim, M. G.; Lee, J. Y.; Cho, J. Green Energy Storage Materials: Nanostructured TiO_2 and Sn-Based Anodes for Lithium-Ion Batteries. *Energy Environ. Sci.* **2009**, *2*, 818−837.
(3) Byoungwoo, K.; Ceder, G. Battery Materials for Ultrafast Charging and Discharging. *Nature* **2009**, *458*, 190−3.
(4) He, M.; Yuan, L.; Hu, X. L.; Zhang, W. X.; Shu, J.; Huang, Y. H. A SnO_2@Carbon Nanocluster Anode Material with Superior Cyclability and Rate Capability for Lithium-Ion batteries. *Nanoscale* **2013**, *5*, 3298−3305.
(5) Ji, L. W.; Zhan, L.; Alcoutlabi, M.; Zhang, X. W. Recent Developments in Nanostructured Anode Materials for Rechargeable Lithium-ion Batteries. *Energy Environ. Sci.* **2011**, *4*, 2682−2699.
(6) Ma, Y.; Ding, B.; Ji, G.; Lee, J. Y. Carbon-Encapsulated F-Doped $Li_4Ti_5O_{12}$ as a High Rate Anode Material for Li^+ Batteries. *ACS Nano* **2013**, *7*, 10870−10878.
(7) Ji, H. X.; Wu, X. L.; Fan, L. Z.; Krien, C.; Fiering, I.; Guo, Y. G.; Mei, Y.; Schmidt, O. G. Self-Wound Composite Nanomembranes as Electrode Materials for Lithium Ion Batteries. *Adv. Mater.* **2010**, *22*, 4591−4595.
(8) Piper, D. M.; Travis, J. J.; Young, M.; Son, S. B.; Kim, S. C.; Oh, K. H.; George, S. M.; Ban, C. Reversible High-Capacity Si Nanocomposite Anodes for Lithium-Ion Batteries Enabled by Molecular Layer Deposition. *Adv. Mater.* **2014**, *26*, 1596−1601.
(9) Sim, S.; Oh, P.; Park, S.; Cho, J. Critical Thickness of SiO_2 Coating Layer on Core@Shell Bulk@Nanowire Si Anode Materials for Li-Ion Batteries. *Adv. Mater.* **2013**, *25*, 4498−4503.
(10) Kasavajjula, U.; Wang, C.; Appleby, A. J. Nano- and Bulk-Silicon-Based Insertion Anodes for Lithium-Ion Secondary Cells. *J. Power Sources* **2007**, *163*, 1003−1039.
(11) Wu, H.; Zheng, G. Y.; Liu, N.; Carney, T. J.; Yang, Y.; Cui, Y. Engineering Empty Space between Si Nanoparticles for Lithium-Ion Battery Anodes. *Nano Lett.* **2012**, *12*, 904−909.
(12) Yu, Y.; Gu, L.; Zhu, C. B.; Tsukimoto, S.; van Aken, P. A.; Maier, J. Reversible Storage of Lithium in Silver-Coated Three-Dimensional Macroporous Silicon. *Adv. Mater.* **2010**, *22*, 2247−2250.
(13) Ng, S. H.; Wang, J.; Wexler, D.; Konstantinov, K.; Guo, Z. P.; Liu, H. K. Highly Reversible Lithium Storage in Spheroidal Carbon-Coated Silicon Nanocomposites as Anodes for Lithium-Ion Batteries. *Angew. Chem., Int.Ed.* **2006**, *45*, 6896−6899.
(14) Zhou, X.; Yin, Y. X.; Cao, A. M.; Wan, L. J.; Guo, Y. G. Efficient 3D Conducting Networks Built by Graphene Sheets and Carbon Nanoparticles for High-Performance Silicon Anode. *ACS Appl. Mater. Interfaces* **2012**, *4*, 2824−2828.
(15) Memarzadeh, E. L.; Kalisvaart, W. P.; Kohandehghan, A.; Zahiri, B.; Holt, C. M. B.; Mitlin, D. Silicon Nanowire Core Aluminum Shell Coaxial Nanocomposites for Lithium ion Battery Anodes Grown with and without a TiN Interlayer. *J. Mater. Chem.* **2012**, *22*, 6655−6668.
(16) Beaulieu, L. Y.; Hatchard, T. D.; Bonakdarpour, A.; Fleischauer, M. D.; Dahn, J. R. Reaction of Li with Alloy Thin Films Studied by In Situ AFM. *J. Electrochem. Soc.* **2003**, *150*, A1457−A1464.
(17) Chen, X.; Li, X. L.; Ding, F.; Xu, W.; Xiao, J.; Cao, Y. L.; Meduri, P.; Liu, J.; Graff, G. L.; Zhang, J. G. Conductive Rigid Skeleton Supported Silicon as High-Performance Li-Ion Battery Anodes. *Nano Lett.* **2012**, *12*, 4124−4130.
(18) Lee, J. K.; Kung, M. C.; Trahey, L.; Missaghi, M. N.; Kung, H. H. Nanocomposites Derived from Phenol-Functionalized Si Nanoparticles for High Performance Lithium Ion Battery Anodes. *Chem. Mater.* **2009**, *21*, 6−8.
(19) Bang, B. M.; Lee, J. I.; Kim, H.; Cho, J.; Park, S. High-Performance Macroporous Bulk Silicon Anodes Synthesized by Template-Free Chemical Etching. *Adv. Energy. Mater.* **2012**, *2*, 878−883.
(20) Liu, N.; Wu, H.; McDowell, M. T.; Yao, Y.; Wang, C. M.; Cui, Y. A Yolk−Shell Design for Stabilized and Scalable Li-Ion Battery Alloy Anodes. *Nano Lett.* **2012**, *12*, 3315−3321.
(21) Wang, B.; Li, X. L.; Zhang, X. F.; Luo, B.; Jin, M. H.; Liang, M. H.; Dayeh, S. A.; Picraux, S. T.; Zhi, L. J. Adaptable Silicon-Carbon Nanocables Sandwiched between Reduced Graphene Oxide Sheets as Lithium Ion Battery Anodes. *ACS Nano* **2013**, *7*, 1437−1445.
(22) Zhu, Y. H.; Liu, W.; Zhang, X. Y.; He, J. C.; Chen, J. T.; Wang, Y. P.; Cao, T. B. Directing Silicon-Graphene Self-Assembly as a Core/Shell Anode for High-Performance Lithium-Ion Batteries. *Langmuir* **2013**, *29*, 744−749.
(23) Yao, Y.; McDowell, M. T.; Ryu, I.; Wu, H.; Liu, N.; Hu, L.; Nix, W. D.; Cui, Y. Interconnected Silicon Hollow Nanospheres for Lithium-Ion Battery Anodes with Long Cycle Life. *Nano Lett.* **2011**, *11*, 2949−2954.
(24) Wang, B.; Li, X. L.; Zhang, X. F.; Luo, B.; Zhang, Y. B.; Zhi, L. J. Contact-Engineered and Void-Involved Silicon/Carbon Nanohybrids as Lithium-Ion-Battery Anodes. *Adv. Mater.* **2013**, *25*, 3560−5.
(25) Song, T.; Xia, J.; Lee, J. H.; Lee, D. H.; Kwon, M. S.; Choi, J. M.; Wu, J.; Doo, S. K.; Chang, H.; Il Park, W.; Zang, D. S.; Kim, H.; Huang, Y.; Hwang, K. C.; Rogers, J. A.; Paik, U. Arrays of Sealed Silicon Nanotubes As Anodes for Lithium Ion Batteries. *Nano Lett.* **2010**, *10*, 1710−1716.
(26) Park, M. H.; Kim, M. G.; Joo, J.; Kim, K.; Kim, J.; Ahn, S.; Cui, Y.; Cho, J. Silicon Nanotube Battery Anodes. *Nano Lett.* **2009**, *9*, 3844−3847.
(27) Wu, H.; Chan, G.; Choi, J. W.; Ryu, I.; Yao, Y.; McDowell, M. T.; Lee, S. W.; Jackson, A.; Yang, Y.; Hu, L.; Cui, Y. Stable Li-ion Battery Anodes by In-Situ Polymerization of Conducting Hydrogel to Conformally Coat Silicon Nanoparticles. *Nat. Nanotechnol.* **2012**, *7*, 309−314.
(28) Yang, Y.; Ren, J. G.; Wang, X.; Chui, Y. S.; Wu, Q. H.; Chen, X.; Zhang, W. Graphene Encapsulated and SiC Reinforced Silicon Nanowires as an Anode Material for Lithium Ion Batteries. *Nanoscale* **2013**, *5*, 8689−8694.
(29) Hwa, Y.; Kim, W. S.; Yu, B. C.; Hong, S. H.; Sohn, H. J. Enhancement of the Cyclability of a Si Anode through Co_3O_4 Coating by the Sol−Gel Method. *J. Phys. Chem. C* **2013**, *117*, 7013−7017.
(30) Li, F.; Yue, H. W.; Wang, P.; Yang, Z. B.; Wang, D. S.; Liu, D. Q.; Qiao, L.; He, D. Y. Synthesis of Core−Shell Architectures of Silicon Coated on Controllable Grown Ni-Silicide Nanostructures and Their Lithium-Ion Battery Application. *CrystEngComm* **2013**, *15*, 7298−7306.
(31) Seh, Z. W.; Li, W. Y.; Cha, J. J.; Zheng, G. Y.; Yang, Y.; McDowell, M. T.; Hsu, P. C.; Cui, Y. Sulphur−TiO_2 Yolk−Shell Nanoarchitecture with Internal Void Space for Long-cycle Lithium-Sulphur Batteries. *Nat. Commun.* **2013**, *4*, 1331.
(32) Lotfabad, E. M.; Kalisvaart, P.; Cui, K.; Kohandehghan, A.; Kupsta, M.; Olsen, B.; Mitlin, D. ALD TiO_2 Coated Silicon Nanowires for Lithium ion Battery Anodes with Enhanced Cycling Stability and Coulombic Efficiency. *Phys. Chem. Chem. Phys.* **2013**, *15*, 13646−13657.
(33) Zhang, J. J.; Wei, Z.; Huang, T.; Liu, Z. L.; Yu, A.-S. Carbon Coated TiO_2−SiO_2 Nanocomposites with High Grain Boundary Density as Anode Materials for Lithium-Ion Batteries. *J. Mater. Chem. A* **2013**, *1*, 7360−7369.
(34) Wei, Z.; Li, R. S.; Huang, T.; Yu, A. S. Fabrication and Electrochemical Properties of Si/TiO_2 Nanowire Array Composites as Lithium Ion Battery Anodes. *J. Power Sources* **2013**, *238*, 165−172.
(35) Zhang, W. M.; Hu, J. S.; Guo, Y. G.; Zheng, S. F.; Zhong, L. S.; Song, W. G.; Wan, L. J. Tin-Nanoparticles Encapsulated in Elastic Hollow Carbon Spheres for High-Performance Anode Material in Lithium-Ion Batteries. *Adv. Mater.* **2008**, *20*, 1160−1165.

(36) Peng, X.; Santulli, A. C.; Sutter, E.; Wong, S. S. Fabrication and Enhanced Photocatalytic Activity of Inorganic Core−Shell Nanofibers Produced by Coaxial Electrospinning. *Chem. Sci.* **2012**, *3*, 1262−1272.
(37) Xu, G. Y.; Ding, B.; Nie, P.; Shen, L. F.; Wang, J.; Zhang, X. G. Porous Nitrogen-Doped Carbon Nanotubes Derived from Tubular Polypyrrole for Energy-Storage Applications. *Chem.—Eur. J.* **2013**, *19*, 12306−12312.
(38) Graetz, J.; Ahn, C. C.; Yazami, R.; Fultz, B. Highly Reversible Lithium Storage in Nanostructured Silicon. *Electrochem.Solid-State Lett.* **2003**, *6*, A194−A197.
(39) Qiao, H.; Wang, Y. W.; Xiao, L. F.; Zhang, L. Z. High Lithium Electroactivity of Hierarchical Porous Rutile TiO_2 Nanorod Microspheres. *Electrochem. Commun.* **2008**, *10*, 1280−1283.
(40) Wang, D.; Choi, D.; Yang, Z.; Viswanathan, V. V.; Nie, Z.; Wang, C.; Song, Y.; Zhang, J. G.; Liu. Synthesis and Li-Ion Insertion Properties of Highly Crystalline Mesoporous Rutile TiO_2. *J. Chem. Mater.* **2008**, *20*, 3435−3442.
(41) Khan, S. U. M.; Al-Shahry, M.; Ingler, W. B. Efficient Photochemical Water Splitting by a Chemically Modified *n*-TiO_2. *Science* **2002**, *297*, 2243−2245.
(42) Hu, Y. S.; Kienle, L.; Guo, Y. G.; Maier, J. High Lithium Electroactivity of Nanometer-Sized Rutile TiO_2. *Adv. Mater.* **2006**, *18*, 1421−1426.
(43) Liu, B.; Aydil, E. S. Growth of Oriented Single-Crystalline Rutile TiO_2 Nanorods on Transparent Conducting Substrates for Dye-Sensitized Solar Cells. *J. Am. Chem. Soc.* **2009**, *131*, 3985−3990.